# On the fluidization/sedimentation velocity of a homogeneous suspension in a low-inertia fluid

Ahmad Amin, Laurence Girolami, Frédéric Risso

# On the fluidization/sedimentation velocity of a homogeneous suspension in a low-inertia fluid

Ahmad Amin[a], Laurence Girolami[a], Frédéric Risso[b]

[a] *Laboratoire GéHCO, Campus Grandmont, Université de Tours, 37200 Tours, France*
[b] *Institut de Mécanique des Fluides de Toulouse (IMFT), Université de Toulouse, CNRS, Toulouse, France*

**Abstract**

The modeling of the fluidization or sedimentation velocity of a suspension of solid particles is revisited by examining experiments conducted in either a liquid or a gas. A general expression is found in the case of negligible fluid inertia, i.e. at low Reynolds or Archimedes number. It is built as the product of the velocity of an isolated particle by three non-dimensional corrections that each takes into account a specific physical mechanism. The first correction reflects the variation of the buoyancy with the particle concentration. The second correction describes how the drag force increases with the concentration in case of negligible particle inertia. The third one accounts for the further increase of the drag when the particle inertia is increased. Remarkably, each correction only relies on a single of the three independent non-dimensional groups that control the problem: (1) the particle volume fraction $\Phi_s$; (2) the ratio $\Phi_s/\Phi_{pack}$ where $\Phi_{pack}$ is the bed packing concentration; (3) the Stokes number $\mathcal{S}t_0$, which characterizes the inertia of the particles and controls their agitation. Moreover, the onset of the instability that separates the homogeneous regime from the heterogeneous one is found to be controlled similarly by the Stokes number. Empirical expressions of the corrections are given, which provide a reliable tool to predict fluidization and sedimentation velocities for all values of the three non-dimensional numbers. The present results emphasize the crucial role of

*laurence.girolami@univ-tours.fr

particle inertia, which is often disregarded in previous modeling approaches, such as that of Richardson and Zaki.
*Keywords:* Fluidization velocity, Sedimentation velocity, Liquid-solid fluidized beds, Gas-solid fluidized beds, Particulate suspensions.

---

## 1. Introduction

This article revisits two closely related fundamental problems: the fluidization of solid particles by an upward flow of fluid and the sedimentation of population of solid particles in a fluid at rest. The physics of these configurations is complex because of the intricate interplay between the continuous fluid phase and the dispersed solid phase. Especially, the interactions between the particles may involve hydrodynamic forces, shocks between particles, solid friction, short-range adhesion forces... In this work, we focus on the case where hydrodynamic forces are predominant, shocks possibly play a significant role, whereas the other effects are negligible. This situation is achieved when the continuous phase is liquid, provided that the particles are not too small to avoid colloidal or Brownian effects, and that their concentration is not too close to packing to avoid solid friction and jamming. It can also be obtained in a gas that is heated in order to prevent capillary forces resulting from moisture. In this context, there exists a range of solid volume fractions in which the flow is homogeneous. Apart from a narrow region close to the wall, the average particle velocity, fluid velocity and volume fraction $\Phi_s$ are spatially uniform. The sedimentation and fluidization processes thus only differ by a Galilean change of reference frame, so that the fluidization velocity $U_f$ and the sedimentation velocity $U_{sed}$ are equal, and will be referred as $U$ in the following of this paper. This range is limited by an upper boundary $\Phi_{up}$ and a lower boundary $\Phi_{low}$. Let us consider a fluidization experiment in which the fluidization velocity is regularly increased while the concentration of the mixture decreases. Concentration $\Phi_{up}$ is reached when the solid friction between the particles ceases to play a significant role and the influence of the walls becomes negligible. It is close to the concentration of the

bed at the minimum fluidization velocity and corresponds to the end of the jamming state. Concentration $\Phi_{low}$ is reached when strong large-scale fluctuations of the particle concentration develop, giving birth to the well-known bubbling regime in gas-solid fluidized beds. Within the homogeneous regime, the dynamics is controlled by four main forces: (1) the effective weight of the particles, which depends on the density difference between the two phases; (2) the viscous stresses within the fluid, which control the dissipation of mechanical energy; (3) the fluid inertial stresses, which influence the flow between the particles; (4) the particle inertia, which determines the intensity of particle-velocity fluctuations relative to those of the fluid. The relative magnitude of these forces depends on the physical parameters that characterize the two phases, which makes it difficult to provide a unified description, valid for a wide range of situations, and to find a universal law capable of describing the relation between $U$ and $\Phi_s$.

Historically, two different ways have been opened to address the problem. The first, initiated by Richardson and Zaki [1, 2] considers the dilute state as a starting point, whereas the second, developed by Abrahamsen and Geldart [3], starts from the packing state.

Let's begin with the Richardson-and-Zaki's approach. The average velocity $U$ is modeled as a correction to the velocity $U_i$ of an isolated settling particle in the corresponding flow regime,

$$U = U_i \left(1 - \Phi_s\right)^n \ , \tag{1}$$

where $n$ is an exponent that is expected to depend on the particle Reynolds number $Re$, being equal to 4.65 in the limit of vanishing $Re$. This approach has become very popular and many studies have shown that eq. 1 describes experimental results well, provided that $U_i$ and $n$ are adequately chosen (see [4] and references therein). Then, several works have investigated how this law can be extended to account for more complex effects, such as suspensions of binary particles [5], adhesion forces depending on temperature [6], magnetic field [7], multisized irregular particles [8]... However, even considering the simplest case of a monodisperse homogeneous suspension of spheres in the absence of

adhesion forces, this approach has limitations. First, eq. 6 predicts that the sedimentation velocity $U$ becomes null at $\Phi = 1$ although it actually vanishes when the jamming occurs, at a concentration which is less than unity. As a consequence, such a law necessarily ceases to be valid when approaching the packing state. On the other hand, the homogeneous regime is destabilized at a concentration $\Phi_{low}$, which is not necessarily small. There is hence no reason to expect that a law that is relevant for $\Phi > \Phi_{low}$ would still be valid in the limit of vanishing concentration, and the value of $U_i$ involved in eq. 6 does not represent the terminal velocity of an isolated settling particle, as it will be shown later. In addition, by following the original dimensional analysis of Richardson and Zaki [2], the proposed expressions for $n$ and $U_i$ [4] generally do not account for the particle inertia, which questions their validity when the particle-to-fluid density ratio can significantly vary from one case to another.

The alternative approach is more specific to the fluidized-bed configuration. The fluidization velocity is modeled as a correction to the minimum velocity $U_{mf}$ required to fluidize the bed [3],

$$U = U_{mf} + \frac{g\,(\rho_s - \rho_f)\,d^2}{210\;\mu_f}\left[\frac{(1-\Phi_s)^3}{\Phi_s} - \frac{(1-\Phi_{pack})^3}{\Phi_{pack}}\right], \qquad (2)$$

where $g$ is the gravitational acceleration, $\rho_s$ the density of the particle, $\rho_f$ the density of the fluid, $d$ the particle diameter, $\mu_f$ the fluid dynamic viscosity and $\Phi_{pack}$ the particle volume fraction of the bed just before expansion. This approach is based on the description of the flow through a porous medium of porosity $\epsilon = 1-\Phi_s$, and can be seen as an extension of the original work of Ergun [9]. Being based on the properties of the bed at $U_{mf}$, it is expected to be relevant at concentrations close to $\Phi_{up}$. But it can hardly constitute a universal law, since its evolution away from $\Phi_{pack}$ does not involve parameters that may account for the variations, between the many possible different fluid/particle systems, of the magnitude of the four main forces listed above. Nevertheless, this approach emphasizes that a model that intends to describe the entire homogeneous regime should probably involve $\Phi_{pack}$.

Suspensions are often described as an equivalent continuous medium of ef-

fective viscosity $\mu_m$. Since the pioneering work of Einstein in 1905, which dealt with the dilute limit, and that of Krieger and Dougherty [10], which proposed a way to continuously connect the dilute and the concentrated regime, many authors have been attempted to model the effective rheology of a suspension (see [11] for a recent review). The definition of an effective viscosity requires to consider a volume that contains enough particles so that the average particle volume concentration can be considered as a relevant parameter at this scale [12]. Consequently, if the effective viscosity is suitable to predict the sedimentation velocity of a large body falling in a suspension of small particles, it is questionable to relate it to the settling velocity of the small particles that make up the suspension. For that reason, although both problems are closely related, the literature on sedimentation/fluidization velocity is disconnected from that on suspension rheology, except in rare cases as [13]. Considering an effective viscosity determined from the mean sedimentation velocity of the particles, which differs from that measured in large-scale sheared suspensions, is however not without interest. This important issue has been recently addressed by two of the authors [14], who defined the effective mixture viscosity $\mu_m$ by balancing the buoyancy force acting on a spherical particle, $g(\rho_s - \rho_f)\frac{\pi}{6}d^3$, to the Stokes drag, $3\pi\,\mu_m\,d\,\frac{U}{1-\Phi_s}$, acting on a particle that moves at velocity $\frac{U}{1-\Phi_s}$ relative to a fluid of viscosity $\mu_m$. This definition turns out to be the only way to gather the experimental values of $U$, measured for three different types of small particles fluidized by a gas, on a master curve of the form

$$\frac{\mu_m}{\mu_f} = \frac{U_0(1-\Phi_s)}{U} = F\left(\frac{\Phi_s}{\Phi_{pack}}\right), \tag{3}$$

where

$$U_0 = \frac{g(\rho_s - \rho_f)d^2}{18\mu_f} \tag{4}$$

is the Stokes velocity for an isolated settling particle, and $F$ is an empirical function that is independent of the nature of the particles. This equation describes non-cohesive fine particles suspended by a gas all over the homogeneous regime. In particular, this law is expected to be valid for fluid catalytic cracking (FCC) or volcanic ash which are both able to generate highly expanded suspensions at

high temperature [15, 16]. However, the question of its generalization to lower particle-to-fluid density ratios, as those corresponding to particles in liquids, remains open and represents the principal objective of this present paper.

In the present work, a fluidization column is used to measure the fluidization and the sedimentation velocities of a suspension of solid particles in a liquid. A series of experiments were carried out for various particle sizes, particle densities and liquid viscosities. Combined with experimental results of our previous work [14] which were performed by using a gas, this amounts to exploring a wide range of the control parameters. From the analysis of these data, we propose an expression able to accurately predict the value of $U$ for any systems involving a suspension of particles all over the homogeneous regime ranging from $\Phi_{low}$ to $\Phi_{up}$, provided that the inertia of the fluid is negligible. This law relies on the key physical parameters that describe the particle/fluid system, namely the Stokes velocity of an isolated particle, the particle volume fraction, a specific packing concentration, and a Stokes number. In addition, the values of $\Phi_{up}$ and $\Phi_{low}$ are also determined and found to be simple functions of the Stokes number, which provides a prediction of the achievable expansion in a fluidization column.

This paper is organized as follows. Section 2 reviews the involved physical parameters and introduces the relevant dimensionless groups. Section 3 describes the experimental setup and presents the investigated systems. Section 4 analyzes the results by means of Richardson-Zaki's and Abrahamsen-Geldart's approaches. Section 5 describes our approach and introduces a new sedimentation/fluidization law. Section 6 examines the boundaries of the homogeneous range. Finally, concluding remarks are given in Section 7.

## 2. Dimensional analysis

We consider the fluidization and the sedimentation of a homogeneous suspension of non-cohesive particles in a fluid. Each particle is characterized by its density $\rho_p$, its equivalent diameter $d = (6\vartheta_p/\pi)^{1/3}$, and its shape. In the case where all particles do not have the same size, we consider that $d$ is either the

mean or median of the diameter distribution. The solid particles are made of a homogeneous material of density $\rho_s$, so that $\rho_p = \rho_s$.

The concentration of the suspension is characterized by the particle (or solid) volume fraction, $\Phi_s$, or equivalently by the fluid volume fraction (or bed porosity), $\epsilon = 1 - \Phi_s$. In order to be able to describe large concentration cases, it is useful to introduce a packing concentration, $\Phi_{pack}$, which is defined as the particle volume fraction of a fluidized bed just below the minimum fluidization velocity or that of a settling suspension at the point where the sedimentation velocity vanishes. Note that, in a fluidized bed, $\Phi_{pack}/\Phi_s$ corresponds to the bed expansion, which can be measured from the ratio between the fluidized bed height and the initial bed height, without knowing the value of $\Phi_{pack}$. It is also worth mentioning that, when considering a population of particles with non-uniform distributions of size and shape, $\Phi_{pack}$ embeds important information about these distributions, which can be enough to determine the sedimentation/fluidization velocity $U$ in certain cases, such as those of heated volcanic ash in a gas [14, 17].

Then, we consider a Newtonian fluid which is characterized by its density, $\rho_f$ and dynamic viscosity, $\mu_f$. Finally, we account for a uniform gravity field of acceleration $g$. Since gravity is only involved in weight and buoyancy, it is better to consider the effective weight $g(\rho_p - \rho_f)$. Also, since the particles are moving relatively to a fluid, it is better to consider their effective inertia, $\rho_p + C_M\rho_f$, where $C_M\rho_f$ represents for the mass of fluid entrained by a particle while $C_M$ is the added-mass coefficient, which is equal to $1/2$ for a sphere.

The problem is thus controlled by seven parameters, two non-dimensional ones ($\Phi_s$, $\Phi_{pack}$) and five dimensional ones ($\rho_f$, $\mu_f$, $d$, $\rho_p + 1/2\rho_f$, $g(\rho_p - \rho_f)$), and involves three physical dimensions (length, mass, time). The problem is thus fully characterized by $7 - 3 = 4$ independent non-dimensional groups. We thus need to build two non-dimensional groups in addition to $\Phi_s$ and $\Phi_{pack}$. Since numerous practical configurations involve fine particles, viscous forces are often dominant. It is thus relevant to introduce non-dimensional numbers that compare inertial forces to viscous ones.

Let us begin by considering the inertia of the fluid. The Reynolds number, $Re = \rho_f dU/\mu_f$, is the non-dimensional group that compares fluid inertial stresses to viscous ones. However, $U$ being not an initial parameter, we need to replace it by a velocity scale that is built on the control parameters. Considering the settling velocity $U_0$ of a single particle in the Stokes regime (Eq. 4), we get the Archimedes number, $\mathcal{A}r = \frac{\rho_f(\rho_p-\rho_f)gd^3}{18\mu_f^2}$.

Evaluating the importance of the particle inertia force is more delicate. Indeed, this force does not play any role when a particle moves at a constant velocity and is therefore associated with the velocity fluctuations that take place in a settling or fluidized suspension. We thus introduce the Stokes number, $\mathcal{S}t = \tau_p/t_f$, which compares the particle response time, $\tau_p$, to the time scale of the fluctuations of the fluid velocity, $t_f$. By balancing particle inertia, $\frac{(\rho_p+1/2\rho_f)\pi d^3 U}{6\tau_p}$ and Stokes drag, $3\pi\mu_f dU$, $\tau_p$ is found to scale with $\frac{(\rho_p+1/2\rho_f)d^2}{\mu_f}$. Then, $t_f$ can be estimated as $d/U$, which leads to $\mathcal{S}t = \frac{(\rho_p+1/2\rho_f)dU}{\mu_f}$. Finally, by replacing $U$ by $U_0$, we obtain a Stokes number that depends only on the initial control parameters: $\mathcal{S}t_0 = \frac{(\rho_p+1/2\rho_f)(\rho_p-\rho_f)gd^3}{18\mu_f^2}$.

The problem is then fully characterized by $\Phi_s$, $\Phi_{pack}$, $Ar$ and $St_0$. Note that $Ar$ is the only non-dimensional group that can be constructed from the three physical parameters when $\rho_p + 1/2\rho_f$ is removed, while $St_0$ is the only one when $\rho_f$ is disregarded. Therefore, in cases where $\mathcal{A}r$ (or $Re$) is small, the inertia of the fluid can be neglected, whereas in cases where $\mathcal{S}t_0$ (or $\mathcal{S}t$) is small, that is the inertia of the particle that is negligible.

## 3. Experimental setup, procedures and regime characterization

We report fluidization and sedimentation experiments that were carried out in the experimental setup schematized in figure 1. It includes a transparent vertical column of height $H = 0.7$ m which has a rectangular cross-section of sides $x_0 = 0.2$ m and $w_0 = 0.3$ m. A liquid, supplied by a centrifugal pump, can be injected at the bottom of the column through an array of straws discharging in a stack of large glass pebbles and smaller lead beads, all covered by a mesh

filter. This injection system ensures a uniform liquid flow and prevents the solid particles from leaving the column. At the top, an evacuation system is connected to an external tank which allows a closed-loop flow.

The experimental procedure can be described as follows. The column is filled with a mixture of solid particles and a liquid. The particles being denser than the liquid, they form a bed of initial height $h_0$. The bed consists of a loose random packing at a concentration $\Phi_{pack}$. The total volume of solid $\vartheta_s$ having been preliminarily measured, the initial concentration is determined as $\Phi_{pack} = \frac{\vartheta_s}{x_0 w_0 h_0}$. Then, the liquid is injected from the bottom at a given flow rate $Q$, corresponding to a fluidization velocity $U_f = \frac{Q}{x_0 w_0}$, determined with an accuracy of $\pm$ 2%. Provided $U_f$ is larger than the minimum fluidization velocity, the bed expands, reaching a height $h > h_0$ and a concentration $\Phi_s$, which correspond to an expansion $E = \frac{h}{h_0}$, determined with an accuracy of $\pm$ 2%. The normalized concentration is thus obtained from $\frac{\Phi_s}{\Phi_{pack}} = \frac{1}{E}$ while the concentration is given by $\Phi_s = \frac{\Phi_{pack}}{E}$, with an accuracy of $\pm$ 4%. When the liquid injection is stopped, the sedimentation velocity is measured from the duration $\Delta t$ taken by the bed to settle: $U_{sed} = \frac{h-h_0}{\Delta t}$, with an accuracy of $\pm$ 4%. A preliminary fluidization-sedimentation cycle is performed before the collect of data, so that the initial packing state $\Phi_{pack}$ is the result of particle sedimentation and not to an arbitrary configuration following the filling of the column. Then, a series of cycles are carried out for different liquid flow rates in order to measure how $U_f$ and $U_{sed}$ evolve with the particle concentration. For each considered system of a fluid and particles, the boundaries $\Phi_{up}$ and $\Phi_{low}$ of the homogeneous regime are determined. Practically, $\Phi_{up}$, is here determined as the concentration corresponding to the minimum flow-rate for which a visible bed expansion is achieved. $\Phi_{low}$ corresponds to the limit of stability of the bed beyond which visible fluctuations of concentration develop and its surface begins to be agitated. Note that this transition is quite abrupt, which makes possible its determination with a good accuracy.

Various systems are investigated (see Table 1 for a summary of their properties). Five sets of particles made of three different solid materials have been

studied, the density of which has been measured by means of a pycnometer: one set of light PMMA beads, three sets of glass beads of different sizes ($GB^1$, $GB^2$ and $GB^3$), and one set of sand grains. Ten samples of each set of particles have been analyzed by using a laser granulometer. Figure 2 shows the distributions of the particle equivalent diameters ($d = (6\vartheta_p/\pi)^{1/3}$). Beside, the shape of the particles was observed using a microscopic image of each sample, also shown in fig. 2. PMMA beads are almost spherical with a narrow size distribution. Glass beads are also almost spherical with a size distribution that is broader for the sets of larger particle sizes. Sand particles are less spherical and have a rather broad size distribution. In what follows, the particle size of each set will be characterized by the median diameter $d_{50}$ of the distribution, we will thus be assimilated to $d$. In any case, the liquid is water but two different operating temperatures are used in order to vary the viscosity: $\mu_l$=1.00×$10^{-3}$ Pa s at 20°C or $\mu_l$=0.72×$10^{-3}$ Pa s at 35°C.

In addition to these new experiments, the present analysis will also consider results obtained in a recent study [14]. This previous work investigated two sets of non-spherical ash particles ($Ash^1$ and $Ash^2$) and one set of almost spherical FCC particles, which were fluidized in air at 170°C [15]. The physical parameters of these experiments are also reported in Table 1. Even though two different setups are used, the experimental procedures of the previous and present experimental campaigns are similar and their results can thus be compared without limitations. Combining results obtained in either a liquid or a gas allows us to explore a very broad range of the Stokes number and thus to reveal the role of the particle inertia.

Figure 3 shows the measured fluidization velocity $U_f$ and sedimentation velocity $U_{sed}$ as a function of the normalized concentration $\frac{\Phi_s}{\Phi_{pack}}$ over the whole range of the stable homogeneous regime between $\frac{\Phi_{low}}{\Phi_{pack}}$ and $\frac{\Phi_{up}}{\Phi_{pack}}$ for all the systems under investigation. In all cases, $U_f$ and $U_{sed}$ are equal within the measurement accuracy, which confirms that wall effects are negligible. In what follows, we will no longer distinguish them and consider a single velocity $U$, the value of which is set equal to the sedimentation velocity $U_{sed}$. Velocity $U$ decreases with

the concentration, but depending on the system under consideration, its values differ greatly. In particular, light PMMA particles in water feature the lowest values, the weakest decrease and the broader homogeneous range, whereas the reverse is true for particles in gas. Considering non-dimensional quantities is therefore necessary to interpret the results.

Table 1 gives the non-dimensional control parameters $\mathcal{A}r$ and $\mathcal{S}t_0$ for all sets of solid particles in water at 20°C and in air at 170°C. The Archimedes number remains moderate ($\mathcal{A}r < 30$) while the Stokes number reaches very large values ($\mathcal{S}t_0$ >1000). Disparities between the values of $U$ of the different fluid-and-particle systems are thus rather expected to be associated with variations of particulate inertia than to fluid one. However, since $\mathcal{A}r$ and $\mathcal{S}t_0$ are based on the Stokes velocity $U_0$ of an isolated settling particle, it is not straightforward to determine the flow regime within a concentrated suspension from their values. This can be better done by examining the Reynolds number $Re$ and the Stokes number $\mathcal{S}t$ which are based on the actual velocity $U$ corresponding to each concentration. Figure 4 shows the evolution of $Re$ and $\mathcal{S}t$ with the normalized concentration. For comparison purposes, the value of $\mathcal{A}r$ (respectively $\mathcal{S}t$) corresponding to each fluid-and-particle system are reported at $\frac{\Phi_s}{\Phi_{pack}} = 0$ in fig. 4a (respectively in fig. 4b).

The maximal value of $Re$, which is reached for the largest glass beads in water at 35°C and at a concentration $\frac{\Phi_s}{\Phi_{pack}}$ around 0.6, is about 4. The classic Schiller and Nauman correlation [18] predicts that the terminal velocity of a solid sphere falling at $Re = 4$ is only decreased by 17% compared to the case at $Re$=0. Furthermore, it must be taken into account that the particles are not isolated, but immersed in a suspension whose effective viscosity $\mu_m$ is higher than that of the suspending fluid. As we will see later in this paper, $\mu_m/\mu_f$ is about 10, which leads to an effective particle Reynolds number less than 0.4 and a velocity decrease from the Stokes value by less than 4%. However, we will observe, in the limit of small concentrations, a reduction of the sedimentation or fluidization velocity relative to the Stokes velocity by a factor of 3 for the cases at the lowest Reynolds number ($Re$=0.004). In these experiments, it is therefore reasonable

to conclude that fluid inertia plays a minor role regarding the fluidization or sedimentation velocity. We will thus disregard the Archimedes number in our analysis of the results

Varying the particle-to-fluid density ratio from 1.2, for PMMA particles in water, to more than 2000, for ash particles in hot air, allows us to investigate an unprecedented range of Stokes numbers ($1.6 \leq St_0 \leq 1200$, $0.015 \leq St \leq 70$) while keeping a low Reynolds number. Little is known about the effect of the Stokes number on the fluidization or sedimentation velocity, so that it is difficult to foresee whether this range is large enough to reveal the whole evolution of $U(St_0)$. It is indeed one of the main objective of this work to investigate this effect in situations where the fluid inertia plays a negligible role.

In the following, we will therefore examine the data by considering the three non-dimensional groups: $\mathcal{S}t_0$, $\Phi_s$ and $\Phi_{pack}$. This choice will be proved to be relevant since all data can be modeled by accounting for these only three parameters.

## 4. Discussion of existing laws

In this section, we confront the two classical approaches with our results. We begin with that of Abrahamsen and Geldart. Fig. 5 compares the predictions of eq. 2 with experimental results. Eq. 2 involves a free parameter that is the minimum fluidization velocity $U_{mf}$ for which we used the value of $U_f$ measured at $\Phi_{up}$, so that experiments and predictions necessarily match at this concentration. For particles in gas, Eq. 2 follows rather the evolution of $U$ at high concentrations. However, it fails at low concentrations and is clearly not suitable for particles in water. Therefore, we do not think that this approach is relevant to gather the data, obtained from configurations of contrasted properties, into a unique description.

Now we examine the popular approach of Richardson and Zaki. Eq. 6 involves two parameters: velocity $U_i$ and exponent $n$. As it is usually done, the experimental results have been represented in Fig. 6a under the form $\log_{10}(\frac{U}{U_i})$

as a function of $\log_{10}(1-\Phi_s)$. The value of $U_i$ corresponding to each experimental system has been determined such that the extrapolation of the best fit of the data by Eq. 6 intercepts $\frac{U}{U_i} = 1$ at $\Phi_s = 0$. Fig. 6a shows that the data of all systems gather on a straight line of slope $n = 3.75$ within values of $\log_{10}(1-\Phi_s)$ ranged from approximately -0.3 to -0.05. This exponent is expected to depend on the Reynolds number. Since the exponent turns out to be the same for all considered systems, which include some cases at very low $Re$, the value found here should correspond to the low-$Re$ limit. However, the present value $n = 3.75$ is significantly lower than the low-Re value $n = 4.65$ proposed by Richardson and Zaki. This is nevertheless not so surprising since, as pointed by [4], various exponents have been reported in the literature. Fig. 6b shows the values of $U_i$, normalized by the Stokes velocity $U_0$ of an isolated settling particle, as a function of $\mathcal{S}t_0$. They are observed to vary from 0.3 $U_0$ to $0.6U_0$ depending on the system under consideration. According to Richardson and Zaki, $U_i$ can be affected by the column dimension or the Reynolds number. Here the ratio $x_0/d$ between the minimum column side and the particle diameter is between 600 and 3000, which is enough to ensure that the results are independent of this parameter. By the way, it is worth mentioning that the existence of a dependence of $U$ on the column dimension is incompatible with the homogeneity of the flow in the transverse direction. Regarding the Reynolds number, we note that the gas cases show the largest deviations to the Stokes velocity although they correspond to the lowest $Re$, which is much less than unity. On the other hand, $\frac{U_i}{U_0}$ can be described as a regular monotonous function of $St_0$, which indicates that, in agreement with the flow regime characterization presented in the previous section, particle inertia is the main cause of discrepancy between the various systems. Yet, the inertia of a particle does not affect its motion when moving at a constant speed. It is thus clear that the value of $U_i$ that allows the results to gather do not correspond to the velocity of an isolated particle. To conclude, the Richardson-Zaki approach, with an appropriate value of $n$ and a value of $U_i$ which depends on $St_0$, allows us to model the present results, provided that we renounce to describe the evolution of $U$ at too small or large concentrations.

## 5. A more universal approach

Our objective is to gather the results obtained for all systems of materials over the entire homogeneous regime. We reconsider the idea presented in our previous study [14] that dealt with solid particles in a gas and thus was limited to high Stokes numbers. Let us consider that the mixture of fluid and particles seen by an individual test particle of diameter $d$ can be considered as a homogeneous fluid of density $\rho_m$ and viscosity $\mu_m = \mu^* \mu_f$. The force balance on a test spherical particle settling at velocity $U$ under the action of gravity within in this fluid is, in the regime of negligible fluid inertia,

$$\frac{\pi d^3}{6}(\rho_p - \rho_m)g = 3\pi\mu^*\mu_f dU \,. \tag{5}$$

Knowing that the mixture density is of $\rho_m = \Phi_s\rho_p + (1-\Phi_s)\rho_f$ and introducing the Stokes velocity $U_0$ of an isolated particle (Eq. 4), leads to

$$\frac{U_0(1-\Phi_s)}{U} = \mu^* \left( \mathcal{S}t_0, \Phi_s, \frac{\Phi_s}{\Phi_{pack}} \right) . \tag{6}$$

This non-dimensional number a priori depends on the three non-dimensional control parameters. It describes the excess of viscous friction acting on the test particle due to the presence of the other particles. It is therefore greater than unity. It tends towards one in the dilute limit and diverges towards infinity when $\Phi_s$ tends toward $\Phi_{pack}$. It is also expected to increase with $\mathcal{S}t_0$ from what we saw in Fig. 6b.

Fig. 7 shows experimental values of the non-dimensional viscosity $\mu^* = \frac{U_0(1-\Phi_s)}{U}$, and its inverse the non-dimensional velocity $U^* = \frac{U}{U_0(1-\Phi_s)}$, as a function of $\frac{\Phi_s}{\Phi_{pack}}$. Even if they contain the same information, these two representations are complementary. The evolution of $\mu^*$ emphasizes the differences between the various cases at large concentrations, while that of $U^*$ highlights the differences at low concentration. Each system of materials is characterized by a specific value of the Stokes number $\mathcal{S}t_0$. We remark that the evolution of $\mu^*$ or $U^*$ against $\frac{\Phi_s}{\Phi_{pack}}$ looks similar at all $\mathcal{S}t_0$. The only differences lie in their overall magnitude and the limit of stability of the homogeneous regime. The

values of $\mu^*$ corresponding to solid particles in a gas are above the others and defined on a short range, whereas those corresponding to PMMA particles in water are below and defined on a very broad range. Comparing all systems, we can claim that the smaller $\mathcal{S}t_0$, the smaller $\mu^*$ and $\Phi_{low}$. A closer look reveals that, over their definition range, the curves are proportional and only differ by a factor, which depends only on $\mathcal{S}t_0$. It means that there exist a function $\mathcal{K}(\mathcal{S}t_0)$ so that the evolutions of $\frac{\mu^*}{\mathcal{K}}$ can be described by a unique function of $\frac{\Phi_s}{\Phi_{pack}}$. The expression of $\mu^*$ thus simplifies into

$$\mu^*\left(\mathcal{S}t_0, \Phi_s, \Phi_{pack}\right) = \mathcal{K}\left(\mathcal{S}t_0\right)\mathcal{F}\left(\frac{\Phi_s}{\Phi_{pack}}\right), \tag{7}$$

where the Stokes number and the concentration are now involved in two separate functions, and where $\Phi_s$ and $\Phi_{pack}$ only appear through their ratio. The experimental values of $\mathcal{K}$ are easily determined from the data. Since it does not depend on the concentration, we can chose any given value $\Phi^*$ of $\frac{\phi_s}{\phi_{pack}}$ to calculate them. The $\mathrm{i}^{th}$ value is given by

$$\mathcal{K}(\mathcal{S}t_0^i) = c\,\frac{\mu^*\left(\mathcal{S}t_0^i, \Phi^*\right)}{\mu^*\left(\mathcal{S}t_0^1, \Phi^*\right)}, \tag{8}$$

where $c$ is a constant that can be arbitrarily included in $\mathcal{K}$ or $\mathcal{F}$ without changing their product, and thus without changing the value of $\mu^*$ according to Eq. 7. We choose the value of $c$ so that $\mathcal{F}$ tends towards unity when $\left(\frac{\Phi_s}{\Phi_{pack}}\right)$ tends toward zero. Fig. 8 represents the experimental data in the form of $\mathcal{F}\left(\frac{\Phi_s}{\Phi_{pack}}\right)$. The corresponding values of $\mathcal{K}(\mathcal{S}t_0)$, obtained by using Eq. 8, are shown in Fig. 9.

The excellent collapse of all data into a unique master curve seen in Fig. 8 proves the validity of the simple model expressed by Eq. 7. In the absence of a theory predicting the function $\mathcal{F}$, it is interesting to search for an empirical expression. It turns out that it cannot be accurately described by either a power law or an exponential function. In fact, the low concentration range shows an exponential increase, whereas the divergence at high concentration is well described by a power law. These considerations lead us to propose an expression of the form

$$\mathcal{F}\left(\frac{\Phi_s}{\Phi_{pack}}\right) = C_0\left(\exp\left[-C_1\left(1-\frac{\Phi_s}{\Phi_{pack}}\right)\right] + C_2\left(1-\frac{\Phi_s}{\Phi_{pack}}\right)^{-C_3}\right), \tag{9}$$

where the constants $C_i$ are positive numbers and $C_0 = \frac{1}{\exp(-C_1)+C_2}$. This expression satisfies the two conditions $\mathcal{F}(0) = 1$ and $\mathcal{F}(1) = \infty$. The best fit is obtained with $C_1 = 3$, $C_2 = 0.08$ and $C_3 = 2/3$. It is represented by the pink curve in Fig. 8 and accurately describes the experimental results.

The evolution of $\mathcal{K}$ against $\mathcal{S}t_0$, plotted in Fig. 9, reveals the effect of the particle inertia on the fluidization or sedimentation velocity. The experimental results show that $\mathcal{K}(\mathcal{S}t_0)$ is an increasing function, with a slope that is large at low $\mathcal{S}t_0$ but then decreases continuously as $\mathcal{S}t_0$ increases, finally reaching a plateau at high $\mathcal{S}t_0$. Such a behavior can be described by means of a simple saturation function of the form

$$\mathcal{K}\left(\mathcal{S}t_0\right) = \left(K_\infty - K_0\right) g\left(\mathcal{S}t_0\right) + K_0\,, \tag{10}$$

where $K_0$ and $K_\infty$ are respectively the limits of $\mathcal{K}\left(\mathcal{S}t_0\right)$ at zero and infinity.

$$g(x) = \frac{x}{x+1}\,, \tag{11}$$

where $x = \frac{\mathcal{S}t_0}{\mathcal{S}t_{0c}}$, $\mathcal{S}t_{0c}$ characterizing the rate at which transition between small and large $\mathcal{S}t_0$ regimes occurs. Now recall that the smaller $\mathcal{S}t_0$, the smaller $\Phi_{low}$. With light particles, dilutions strong enough for $U$ to approach $U_0$ can be achieved while remaining in the homogeneous regime. Thus, if we stand that $\Phi_{low}$ tends towards zero when $\mathcal{S}t_0$ tends towards zero, we obtain from Eqs. 6 and 7

$$\mu^*\left(\mathcal{S}t_0 = 0, \frac{\Phi_{low}}{\Phi_{pack}}\right) = \mu^*\left(0,0\right) = K_0\mathcal{F}(0) = K_0 = \frac{U_0(1-0)}{U_0} = 1\,. \tag{12}$$

Given that $K_0 = 1$, $K_\infty$ and $\mathcal{S}t_{0c}$ are the two remaining free parameters in Eq.10. A reasonable fit of the experimental results, shown by the pink curve in Fig. 9, is obtained by setting $K_\infty = 3$ and $\mathcal{S}t_{0c}$=45. (It can be mentioned that a slightly better fit of the experimental results is obtained with $K_0 = 1.5$, $K_\infty = 3$ and $\mathcal{S}t_{0c}$=70, but is not consistent with equation 12.)

We finally end up with a general model of the sedimentation/fluidization velocity $U$ of a suspension that is valid all over the homogeneous range and for all systems of fluid and particles, provided that the inertia of the fluid can be

neglected compared to viscous forces. From Eqs. 6 and 7, $U$ can be written as a product of four terms

$$U = \underbrace{\frac{g(\rho_p - \rho_f)d^2}{18\ \mu_f}}_{\text{1. Isolated particle, } U_0} \underbrace{(1-\phi_s)}_{\text{2. mixture density}} \underbrace{\frac{1}{\mathcal{F}\left(\frac{\phi_s}{\phi_{pack}}\right)}}_{\text{3.bed porosity, Eq. 9}} \underbrace{\frac{1}{\mathcal{K}\left(\mathcal{S}t_0\right)}}_{\text{4. particle agitation, Eq. 10}}, \tag{13}$$

which can be interpreted as follows:

1. The first term is the theoretical Stokes terminal velocity $U_0$ of an isolated sphere of density $\rho_p$ settling under the action of gravity in a fluid of density $\rho_f$ and viscosity $\mu_f$. It is the value reached by $U$ when both $\Phi_s = 0$ and $\mathcal{S}t_0 = 0$. The three other terms are non-dimensional corrections to $U_0$ accounting for the various effects associated with the presence of many particles.

2. The second term simply accounts for the evolution of the density $\rho_m$ of the mixture which affects the buoyancy force acting on each solid particle in Eq. 5. As noticed in [14], Eq. 5 can also be obtained by considering a test particle moving at velocity $\frac{U}{1-\Phi_s}$ relative to the fluid of density $\rho_f$ instead of moving at velocity $U$ relative to the mixture of particles and fluid at density $\rho_m$. Thus, the second term can also be interpreted as reflecting the increase of the relative velocity between the particle and the fluid when the concentration increases. It is worth mentioning that this term is not associated with interactions between particles nor with an increase of the drag force acting on the particles.

3. As well as in a porous medium, the fluid follows complex paths within the interstices between the particles. The friction on each particle and the corresponding viscous dissipation are therefore increased compared to the case of an isolated particle. This causes the increase of the average drag force on the particle and the decrease of $U$. The third term of Eq. 13, modeled by Eq. 9, quantifies this effect in the case of particles of negligible inertia, i.e. $\mathcal{S}t_0 = 0$. Function $\frac{1}{\mathcal{F}}$ decreases from unity to zero as $\frac{\phi_s}{\phi_{pack}}$ goes from zero (isolated particle) to one (packed state).

4. In fluidized beds or sedimenting suspensions, both fluid and particle velocities undergo fluctuations, even at low Reynolds number [19, 20]. These fluctuations contribute to the dissipation of mechanical energy and thus affect the average velocity $U$. In particular, the fluctuations of the relative velocity between the fluid and the particles are intimately related to how $U$ depends on the concentration [21]. However, these fluctuations do not only depend on the concentration but also on the Stokes number. Particles of negligible inertia ($\mathcal{S}t_0 \ll 1$) instantaneously follow any local fluctuations of the fluid that surrounds them, while particles of significant inertia follow trajectories that differ from those of the fluid. For particles of negligible inertia, the effect of the fluctuations is already embedded in $\frac{1}{\mathcal{F}}$ and turns out to vanish at strong dilution. The fourth term of Eq. 13, modeled by Eq. 10, describes the evolution of this effect with the Stokes number. It turns out that $\frac{1}{\mathcal{K}}$ is a decreasing function of $\mathcal{S}t_0$ which reaches a minimum value of about 1/3 at large $\mathcal{S}t_0$. The larger $\mathcal{S}t_0$, the smaller $U$, which is at most three times smaller for high-inertia particles compared to low-inertia ones.

## 6. Boundaries of the homogeneous range

Eq. 13 provides a general relation between $U$ and all the control parameters of the problem. To achieve a complete description, we need henceforth to determine the boundaries of the homogeneous range in which this law is valid.

Fig. 10a shows the upper boundary, $\frac{\Phi_{up}}{\Phi_{pack}}$, as a function of $\mathcal{S}t_0$. Note that $\Phi_{up}$ is defined as the maximum concentration below which the bed of particles is fully fluidized, i.e. $U_f = U_{sed}$. In principle, this point may differ from the concentration $\Phi_{mf}$ corresponding to the minimum fluidization velocity, where the presence of the wall can still play a significant role and cause $U_f$ to be larger than $U_{sed}$. However, it turned out that $U_f$ was approximately equal to $U_{sed}$ at the first point where measurable expansion was detected. We can thus make no distinction between $\Phi_{up}$ and $\Phi_{mf}$ in the present experiments. This is not

surprising since the ratio between $\Phi_{up}$ and $\Phi_{pack}$ remains in any case ranged from 0.94 and 1, without showing any clear correlation with $\mathcal{S}t_0$.

The study of the lower boundary $\Phi_{low}$ is much more interesting, since it characterizes the limit of stability of the homogeneous regime when the concentration is decreased as well as the bed expansion. Above $\Phi_{low}$, the bed shows no noticeable fluctuations. Below $\Phi_{low}$ the surface of the bed becomes strongly agitated and visible fluctuations of concentration at large scales compared to $d$ are visible. Fig. 10b shows $\frac{\Phi_{low}}{\Phi_{pack}}$ as a function of $\mathcal{S}t_0$. It is immediately noticeable that this behavior is similar to that of $\mathcal{K}(\mathcal{S}t_0)$ presented in Fig. 9 and can thus be described by an expression similar to Eq. 10,

$$\frac{\Phi_{low}}{\Phi_{pack}}(\mathcal{S}t_0) = \left( \left[\frac{\Phi_{low}}{\Phi_{pack}}\right]_\infty - \left[\frac{\Phi_{low}}{\Phi_{pack}}\right]_0 \right) g(\mathcal{S}t_0) + \left[\frac{\Phi_{low}}{\Phi_{pack}}\right]_0, \qquad (14)$$

where function $g$ is still given by Eq. 11 with $\mathcal{S}t_{0c}$=45. The best fit of the experimental results, given by $\left[\frac{\Phi_{low}}{\Phi_{pack}}\right]_0 = 0$ and $\left[\frac{\Phi_{low}}{\Phi_{pack}}\right]_\infty = 0.8$, is represented by the pink curve in Fig. 10b. Considered together, the evolutions of $\mathcal{K}(\mathcal{S}t_0)$ and $\frac{\Phi_{low}}{\Phi_{pack}}(\mathcal{S}t_0)$ draw an interesting picture. First, it is worth recalling that $\left[\frac{\Phi_{low}}{\Phi_{pack}}\right]_0 = 0$ means that a bed of particles of negligible inertia should be expanded without limit while remaining homogeneous. At $\mathcal{S}t_0 = 0$, there is no discontinuity between the case of an isolated particle ($\Phi_s = 0$) and the onset of the transition towards jamming ($\Phi_s = \Phi_{pack}$), $U$ being determined by the three first terms of Eq. 13. At $\mathcal{S}t_0 > 0$, the velocity $U$ is divided by a factor $\mathcal{K}(\mathcal{S}t_0) > 1$ and, concurrently, the homogeneous regime is restricted to concentrations larger than $\Phi_{low}(\mathcal{S}t_0) > 0$. In this case, the existence of a bifurcation at $\Phi_{low}$ limits the evolution of $U$ that cannot be extrapolated towards $\Phi_s = 0$ to recover the value $U_0$ corresponding to an isolated particle. Increasing $\mathcal{S}t_0$ leads to the increase of $\mathcal{K}$ and $\frac{\Phi_{low}}{\Phi_{pack}}$ by following a similar law, which indicates that the same mechanism related to the inertia of the particles is responsible for both the instability of the suspension and the decrease of $U$.

## 7. Conclusion

From a thorough examination of experimental results conducted with systems of contrasted properties, we have established a general law (Eq. 13) for the sedimentation/fluidization velocity $U$ of a non-cohesive suspension of particles in a low-inertia fluid, either gaseous or liquid. This law takes into account all the physical parameters that control the flow. It is valid over the whole range of particle volume fractions where a fully fluidized homogeneous suspension is stable, between the lower limit $\Phi_{low}$ below which large-scale fluctuations of concentration develop, and the upper limit $\Phi_{up}$ above which solid friction starts to play a significant role. A major finding of this work is that the expression of $U$ can be decomposed into the product of four terms, each of them accounting for a different physical mechanism: (1) the settling velocity of an isolated particle, (2) the effective particle weight, (3) the effect of the concentration of particles of negligible inertia (4) the effect of particle inertia. Remarkably, the function $\mathcal{F}\left(\frac{\Phi_s}{\Phi_{pack}}\right)$ modeling term (3) is independent of function $\mathcal{K}\left(\mathcal{S}t_0\right)$ modeling term (4). Also, the flow instability beyond a given concentration is directly related to the inertia of the particles. A bed of inertialess particles ($\mathcal{S}t_0 = 0$) can be indefinitely expanded while remaining stable. Increasing $\mathcal{S}t_0$, $\frac{\Phi_{low}}{\Phi_{pack}}$ and $\mathcal{K}\left(\mathcal{S}t_0\right)$ both increase by following the same law. Thus, the larger the Stokes number, the lower $U$ and the less the maximum stable bed expansion.

Combined to general expression 13, empirical laws 9, 10 and 14 provide a reliable tool for engineers needing to predict the behavior of a fluidized bed. Note that this expression is valid in the homogeneous regime and cannot be extrapolated to values of $\Phi_s$ that are lower than $\Phi_{low}$.

Now, let us discuss two possible limitations of the present result. We can wonder whether there could be an effect of the width of the size distribution. Although the particle sets investigated in a liquid (Fig. 2) as well as those investigated in a gas (Fig. 1 of [16], [14]) have various size distributions, our model is able to describe them by only accounting for the average diameter of the particles. We thus think that the particle distribution can be disregarded, provided

that its width is narrow enough to prevent size segregation from occurring [22]. Note that the mixture was made with the same material and also prevents the density segregation. Moreover, in experiments made in gas, one set of roughly spherical FCC particles and two sets of non-spherical randomly shaped volcanic ash were studied (see pictures in Fig. 1 of [16], [14]). In experiments made in liquid, glass beads and PMMA particles are spherical, whereas sand grains are not (see pictures in Fig. 2). Since the present model is found to work with all the considered materials, it seems that $\Phi_{pack}$ embeds the most important information about the particle shape, at least for shapes that are moderately anisotropic.

Lastly, it is important to recall that the present model described situations where the effect of the fluid inertia can be neglected, i.e. small Reynolds numbers. To deal with all possible cases, a model must provide the dependence of $U$ with all four non-dimensional parameters: $\Phi_s$ and $\Phi_{pack}$, $St_0$ and $Ar$. Is it possible to extend the present model to include the Archimedes number ? A more general expression for the velocity of the isolated particle (term 1) could be considered in oder to account for a finite-Reynolds-number drag. Also, the effect of the concentration on the mixture density (term 2) should remain unchanged. However, it is more difficult to anticipate about the two other terms. In particular, it would be interesting to know whether a separation of variables as that expressed by Eq. 7 is still relevant when the role of $Ar$ is considered. A Future work based on further experimental investigations will address these issues.

**Acknowledgment**

This study was supported by the Region Centre-Val de Loire (Contribution of 'Academic Initiative' : MAGIC/201500103985). LG particularly thanks Romain Morini and Stephane Moreau (AVILEX) for their contribution to experiments.

## References

## References

[1] J. F. Richardson, W. N. Zaki, The sedimentation of a suspension of uniform spheres under conditions of viscous flow, Chemical Engineering Science 3 (2) (1954) 65–73.

[2] J. F. Richardson, W. N. Z. P. D, Sedimentation and fluidisation: Part I, Trans. Inst. Chem. Eng. 32 (1954) S82–S100.

[3] A. R. Abrahamsen, D. Geldart, Behaviour of gas-fluidized beds of fine powders part I. Homogeneous expansion, Powder Technology 26 (1) (1980) 35–46.

[4] O. J. I. Kramer, P. J. de Moel, E. T. Baars, W. H. van Vugt, J. T. Padding, J. P. van der Hoek, Improvement of the Richardson-Zaki liquid-solid fluidisation model on the basis of hydraulics, Powder Technology 343 (2019) 465–478.

[5] N. Funamizu, T. Takakuwa, An improved Richardson-Zaki formula for computing mixed layer composition in binary solid-liquid fluidized beds, Chemical Engineering Science 50 (19) (1995) 3025–3032.

[6] P. Lettieri, D. Newton, J. G. Yates, Homogeneous bed expansion of FCC catalysts, influence of temperature on the parameters of the Richardson–Zaki equation, Powder Technology 123 (2-3) (2002) 221–231.

[7] J. M. Valverde, A. Castellanos, A modified Richardson–Zaki equation for fluidization of Geldart B magnetic particles, Powder Technology 181 (3) (2008) 347–350.

[8] M. Bargieł, E. M. Tory, Extension of the Richardson–Zaki equation to suspensions of multisized irregular particles, International Journal of Mineral Processing 120 (2013) 22–25.

[9] S. Ergun, Fluid flow through packed colmuns, Chemical Engineering Progress 48 (2) (1952) 89–94.

[10] I. M. Krieger, T. J. Dougherty, A mechanism for non-Newtonian flow in suspensions of rigid spheres, Transactions of the Society of Rheology 3 (1) (1959) 137–152.

[11] É. Guazzelli, O. Pouliquen, Rheology of dense granular suspensions, Journal of Fluid Mechanics 852 (2018) 35–73.

[12] E. J. Hinch, An averaged-equation approach to particle interactions in a fluid suspension, Journal of Fluid Mechanics 83 (4) (1977) 695–720.

[13] S. Koo, Sedimentation velocity of bidisperse suspensions, Journal of Industrial and Engineering Chemistry 14 (5) (2008) 679–686.

[14] L. Girolami, F. Risso, Sedimentation of gas-fluidized particles with random shape and size, Physical Review Fluids 4 (7) (2019) 074301.

[15] L. Girolami, Dynamique et sédimentation des écoulements pyroclastiques reproduits en laboratoire, Ph.D. thesis, Université de Clermont II (2008).

[16] L. Girolami, T. H. Druitt, O. Roche, Towards a quantitative understanding of pyroclastic flows: Effects of expansion on the dynamics of laboratory fluidized granular flows, Journal of Volcanology and Geothermal Research (296) (2015) 31–39.

[17] L. Girolami, F. Risso, Physical modeling of the dam-break flow of sedimenting suspensions, Physical Review Fluids 5 (8) (2020) 084306.

[18] R. Clift, J. Grace, M. Weber, Bubble, Drops and Particles, Academic Press, 1978.

[19] N.-Q. Nguyen, A. J. C. Ladd, Sedimentation of hard-sphere suspensions at low Reynolds number, Journal of Fluid Mechanics 525 (2005) 73–104.

[20] M. Abbas, E. Climent, O. Simonin, M. R. Maxey, Dynamics of bidisperse suspensions under Stokes flows: Linear shear flow and sedimentation, Physics Of Fluids 18 (12) (2006) 121504.

[21] E. Alméras, O. Masbernat, F. Risso, R. O. Fox, Fluctuations in inertial dense homogeneous suspensions, Physical Review Fluids 4 (10) (2019) 102301.

[22] J. L. P. Chen, D. L. Keairns, Particle segregation in a fluidized bed, The Canadian Journal of Chemical Engineering 53 (4) (1975) 395–402.

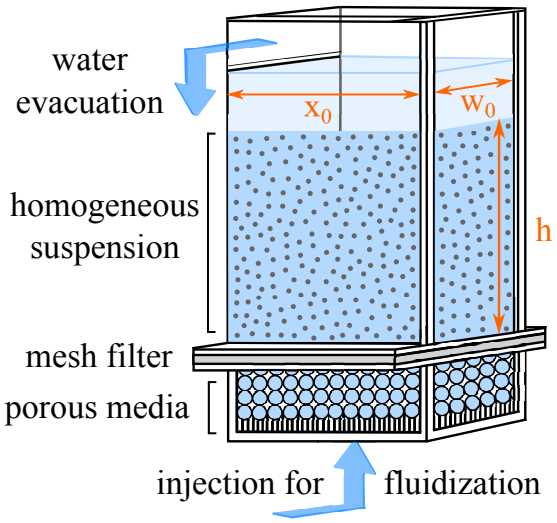


Figure 1: Scheme of the fluidization column.

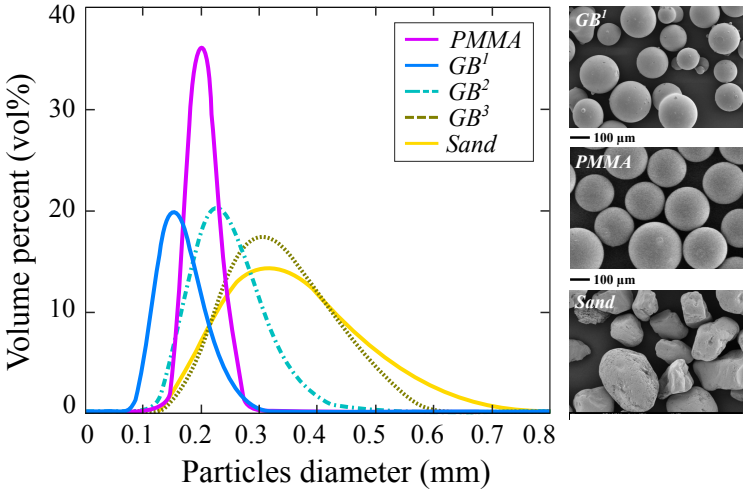


Figure 2: Particle size distribution and microscopic pictures of the materials used in the experiments.

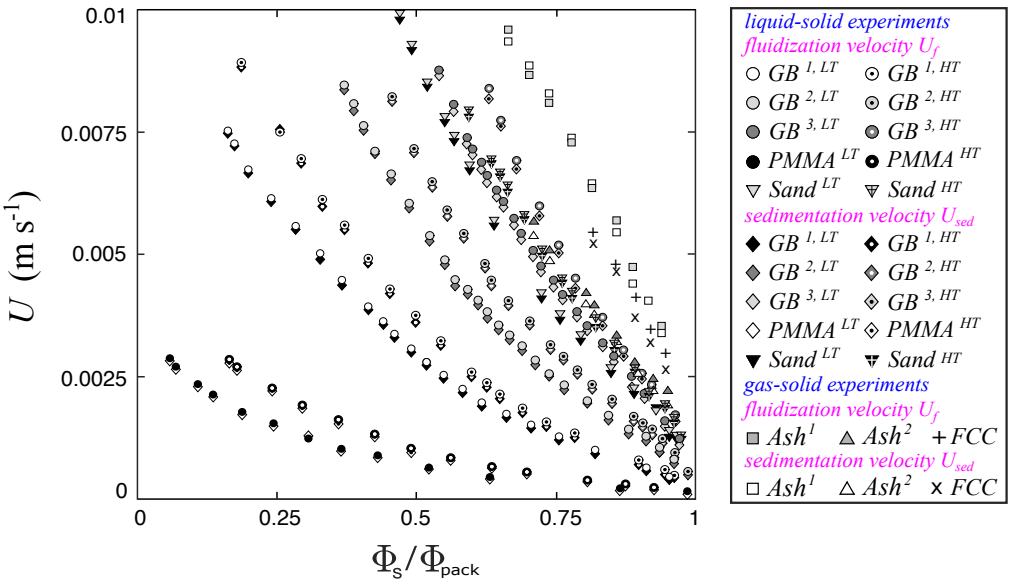


Figure 3: Fluidization velocity $U_f$ and sedimentation velocity $U_{sed}$ represented as a function of the normalized solid particle volume fraction $\frac{\phi_s}{\phi_{pack}}$ for both liquid-solid and gas-solid suspensions.

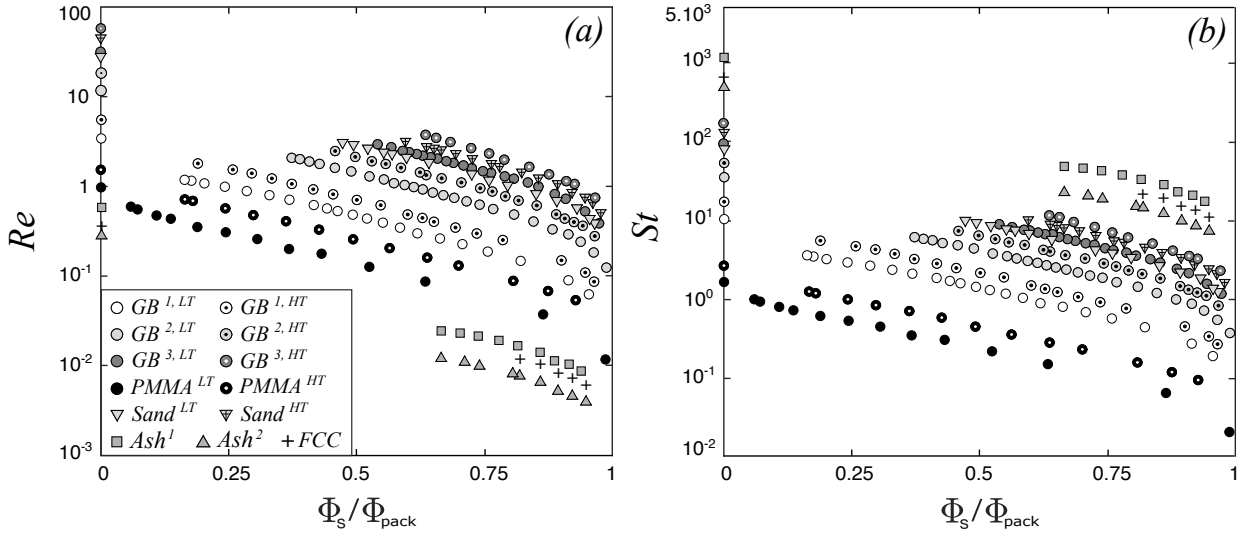


Figure 4: (a) Particles Reynolds number $\mathcal{R}e$ and (b) Stokes number $\mathcal{S}t$ as a function of $\Phi_s/\Phi_{pack}$.

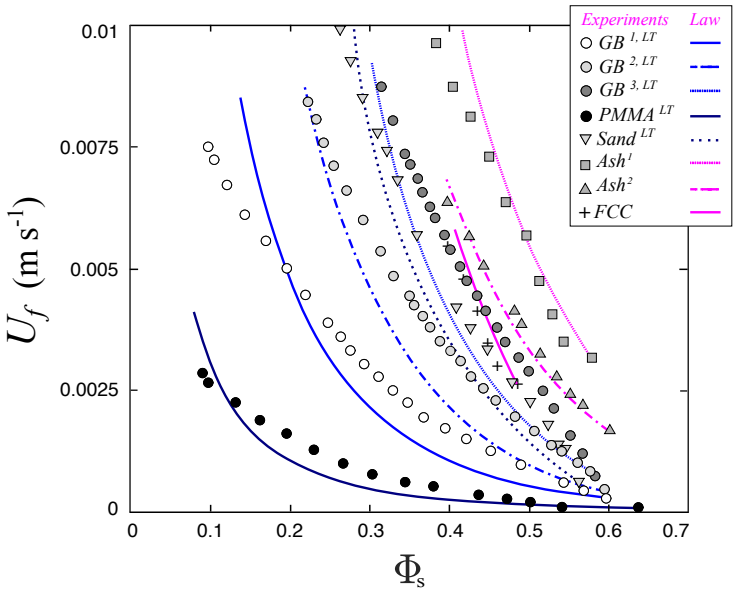


Figure 5: Fluidization velocity $U_f$ as a function of the particle volume fraction $\Phi_s$. Plain lines represent the Abrahamsen-Geldart's [3] (Eq. 2) prediction for both the liquid-solid and the gas-solid suspensions.

| Experimental parameters | $PMMA$ | $GB^1$ | $GB^2$ | $GB^3$ | $Sand$ | $Ash^1$ | $Ash^2$ | $FCC$ |
|---|---|---|---|---|---|---|---|---|
| Particle density $\rho_p$ [kg m$^{-3}$] | 1200 | 2500 | 2500 | 2500 | 2650 | 1600 | 1490 | 1420 |
| Mean particle diameter $d$ [$\mu$m] | 210 | 160 | 240 | 335 | 310 | 80 | 65 | 70 |
| Fluid density $\rho_f$ [kg m$^{-3}$] | 998 | 998 | 998 | 998 | 998 | 0.79 | 0.79 | 0.79 |
| Fluid viscosity $\mu_f$ [Pas] | $10^{-3}$ | $10^{-3}$ | $10^{-3}$ | $10^{-3}$ | $10^{-3}$ | $2.45\,10^{-5}$ | $2.45\,10^{-5}$ | $2.45\,10^{-5}$ |
| Packing concentration $\Phi_{pack}$ | 0.64 | 0.60 | 0.60 | 0.58 | 0.56 | 0.58 | 0.60 | 0.58 |
| Limit of fluidization $\frac{\phi_{up}}{\phi_{pack}}$ | 0.987 | 0.955 | 0.966 | 0.972 | 0.967 | 0.94 | 0.95 | 0.95 |
| Limit of stability $\frac{\phi_{low}}{\phi_{pack}}$ | 0.06 | 0.16 | 0.38 | 0.62 | 0.47 | 0.70 | 0.71 | 0.82 |
| Range of homogeneous regime $\frac{\phi_{up}}{\phi_{low}}$ | 16.45 | 5.97 | 2.54 | 1.80 | 1.57 | 1.34 | 1.34 | 1.16 |
| $\mathcal{A}r = \frac{\rho_f(\rho_p-\rho_f)gd^3}{18\mu_f^2}$ | 1 | 3 | 11 | 31 | 28 | 0.6 | 0.3 | 0.4 |
| $\mathcal{S}t_0 = \frac{(\rho_p-\rho_f)(\rho_s+\frac{1}{2}\rho_f)gd^3}{18\ \mu_f^2}$ | 1.6 | 10 | 34 | 94 | 88 | 1176 | 545 | 655 |

Table 1: Experimental parameters for both liquid-solid suspensions ($PMMA$; $GB^1$; $GB^2$; $GB^3$; $Sand$) at 20$^o$C and gas-solid suspensions ($Ash^1$; $Ash^2$; $FCC$) at 170$^o$C.

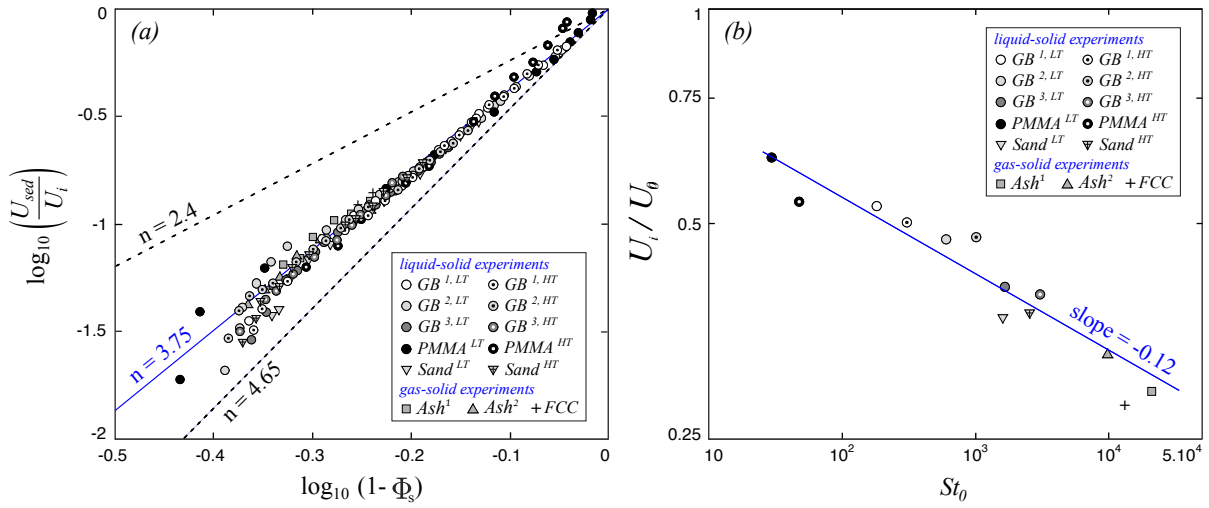


Figure 6: Presentation of the experimental results according to the Richardson and Zaki approach [2] (Eq. 1). (a) Decimal logarithm of the sedimentation velocity, $\log_{10}\left(\frac{U_{sed}}{U_i}\right)$, as a function of that of the bed porosity $\log_{10}(1-\Phi_s)$. The dashed lines correspond to exponents $n = 4.65$ of the low-Re regime and $n = 2.4$ of the high-Re regime. (b) Velocity $U_i$ normalized by the Stokes velocity $U_0$ as function of the Stokes number $\mathcal{S}t_0$.

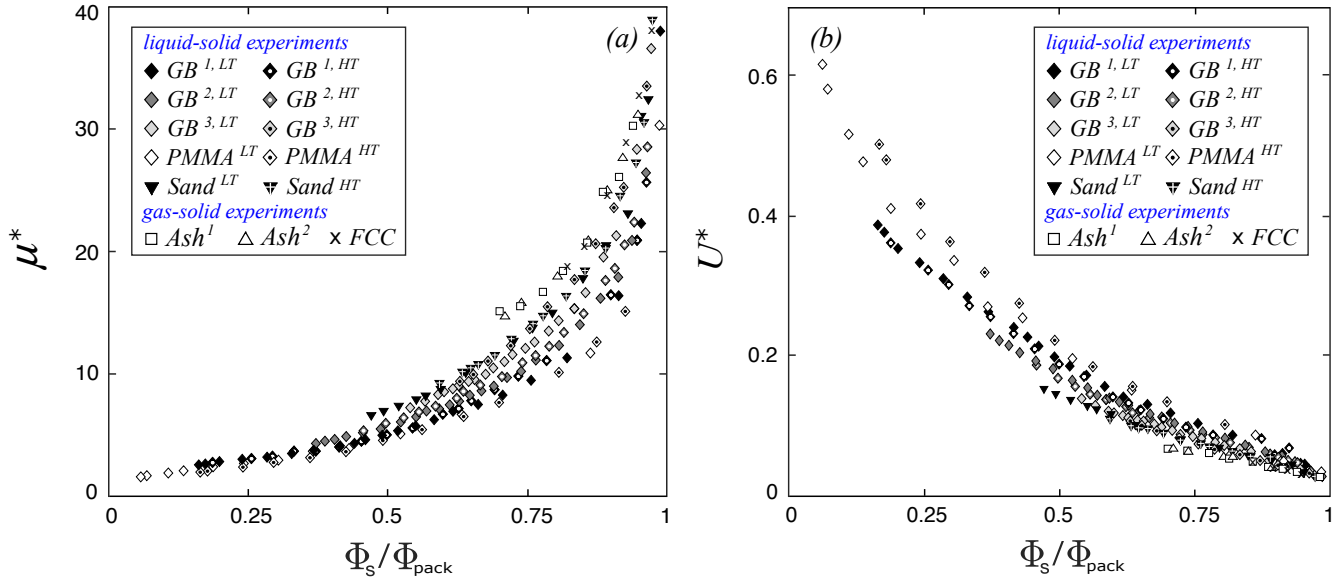


Figure 7: Experimental results on the non-dimensional form $\mu^* = \frac{U_0}{U(1-\Phi_s)}$ or $U^* = \frac{U(1-\Phi_s)}{U_0}$ as a function of $\frac{\Phi_s}{\Phi_{pack}}$.

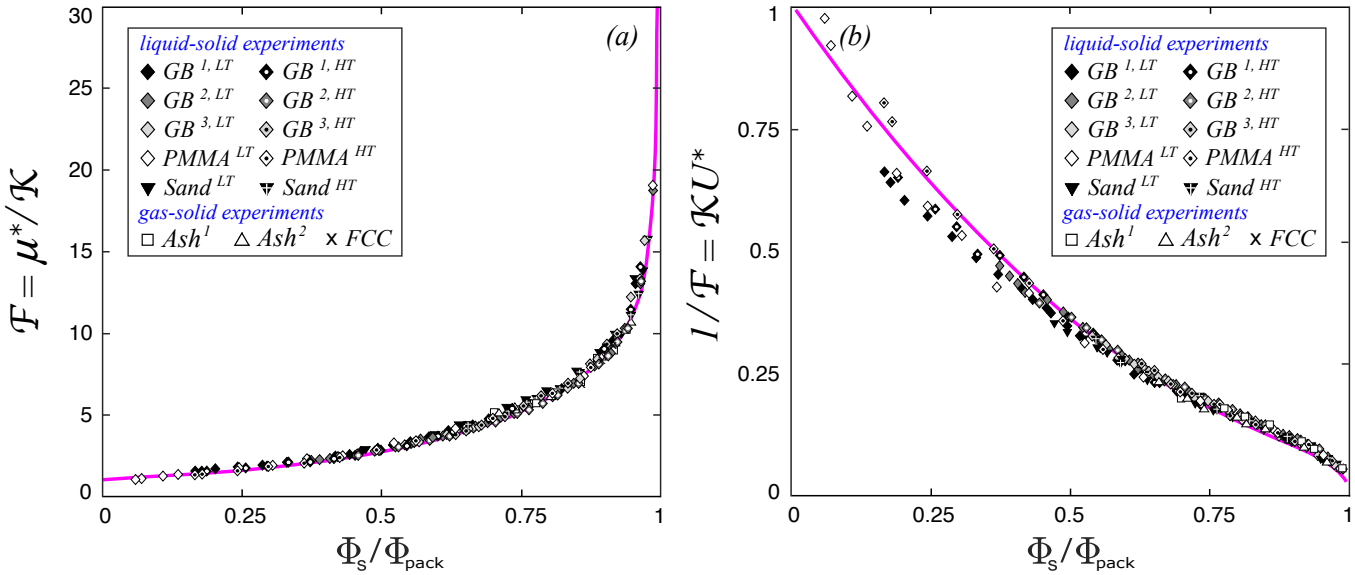


Figure 8: Non-dimensional function $\mathcal{F}\left(\frac{\Phi_s}{\Phi_{pack}}\right) = \frac{\mu^*}{\mathcal{K}(\mathcal{S}t_0)}$, which reflects the dependence of $U$ on the concentration due to the enhanced viscous dissipation in the presence of many particles. Symbols represent experiments, the pink curve shows empirical law 9.

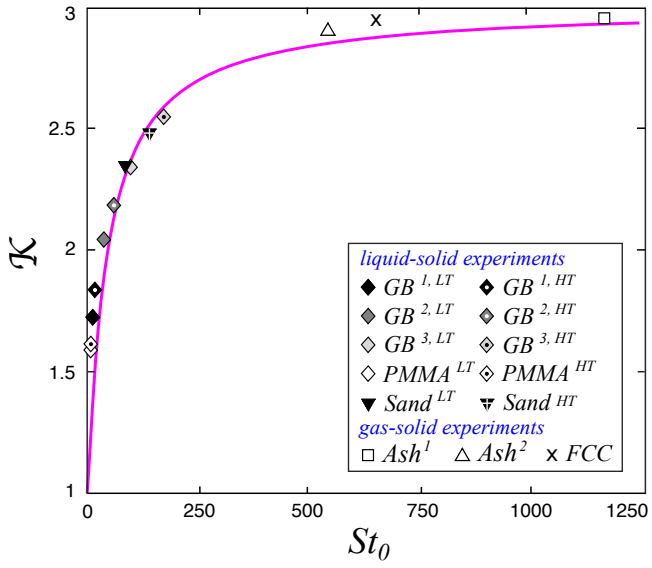


Figure 9: Non-dimensional function $\mathcal{K}(\mathcal{S}t_0)$, which reflects the increase of viscous dissipation due to the difference between instantaneous motions between inertial particles and the carrier fluid. Symbols represent experiments, the pink curve shows empirical law 10.

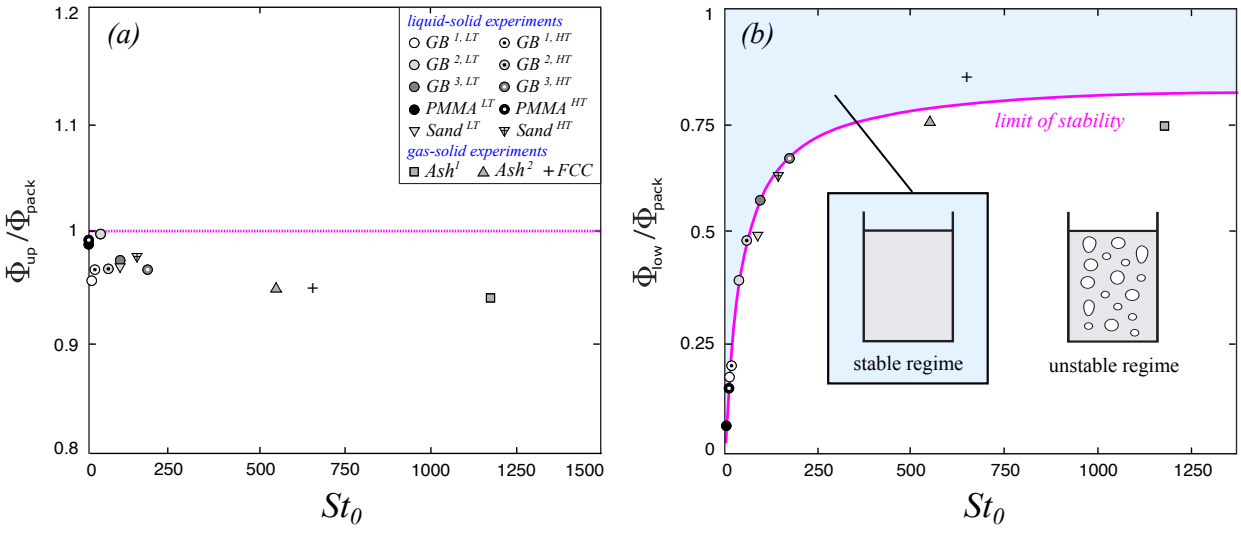


Figure 10: Boundaries of the homogeneous range at a function of $\mathcal{S}t_0$. (a) Upper limit $\left(\frac{\phi_{up}}{\phi_{pack}}\right)$ determined from the minimum fluidization velocity; (b) lower limit $\left(\frac{\phi_{low}}{\phi_{pack}}\right)$ corresponding to the onset of the bed instability.